Magnetoelectric effects and spin switching phenomena at the interface of chiral domains in spin-triplet superconductors

Alfonso Romano, Canio Noce, and Mario Cuoco
Dipartimento di Fisica "E. R. Caianiello," Università di Salerno, I-84084 Fisciano (Salerno), Italy and CNR-SPIN, I-84084 Fisciano (Salerno), Italy

(Received 4 April 2019; revised manuscript received 3 June 2019; published 14 June 2019)

Spin-triplet superconductors with time-reversal symmetry breaking can naturally lead to chiral domain walls in their interior. We study the magnetic properties emerging at the interface of chiral domains with opposite winding by focusing on the effects of a superconducting phase drop across the wall and an applied electric gating. The local inversion symmetry breaking at the domain wall drives mixed singlet-triplet pairing configurations that allow a phase- and electric-controllable magnetization with resulting parallel or antiparallel orientations on the two sides of the domain wall. The magnetic switching is also generally accompanied by both spin and charge currents flowing along the edges, whose amplitudes depend on the achieved parallel or antiparallel magnetic phase. The specific magnetoelectric properties of chiral domains with zero or nonvanishing net magnetization near the wall may have several implications. They can be employed to detect the presence of unconventional pairing as well as to design information storage units based on spin-polarized states attached to topological defects.

DOI: 10.1103/PhysRevB.99.224507

I. INTRODUCTION

The coherent control and manipulation of the electron spin in superconducting heterostructures set the basis for fundamental challenges in solid-state physics which point, among the large variety of emerging effects, towards the implementation of outperforming energy-efficient spintronics devices. In superconducting materials, the Cooper pairs can form coherent states both in the conventional s-wave spin-singlet channel and with spin-1 angular momentum and orbital p-wave symmetry [1–8]. In the latter case, the order parameter has both orbital and spin-active degrees of freedom, which can lead to a nonstandard response to Zeeman/ferromagnetic fields [9–16], spin-sensitive Josephson transport [17–22], and superconducting spintronics [23]. The previous phenomena are representative cases of a large class of effects where the character of the order parameter and the interface play a primary role in determining the symmetry and the nature of the emerging electronic states. Indeed, interface electronic reconstructions are typically responsible for unconventional proximity effects, edge states, and possible spontaneous symmetry breaking as well as unusual spin and charge electronic transport.

Among the various superconducting systems, of special relevance are those with nontrivial topological properties. This is the case, for instance, of the two-dimensional chiral $(p + ip)$-wave superconductor with a time-reversal symmetry-breaking order parameter, as realized in the Sr_2RuO_4 compound [7,24–26]. A distinctive element of these spin-triplet phases is that the topological nature arises from the orbital degeneracy of the superconducting order parameter, for example, between p_x and p_y states, allowing for the existence of different types of domains (e.g., $p_x \pm ip_y$). Since we are dealing with an Ising-type degeneracy and the superconducting state has only two possible configurations, the domain walls separating such regions are well defined in space, and near the wall, the order parameter exhibits spatial gradients that give rise to in-gap electronic states [27]. Chiral p-wave superconductivity can generally occur in two possible topological configurations with clockwise or counterclockwise winding of the orbital component for each spin orientation [28], thus allowing for two types of chiral domains separated by a domain wall (DW) (see Fig. 1). Direct evidence of the occurrence of chiral DW [29] is still controversial and elusive, although there have been several observations which refer to its manifestation, for instance, indicated by transport studies in Sr_2RuO_4 junctions [30–32]. Such a domain wall has also been proposed as an observable channel of nonzero conductance measured between a pair of metal contacts [33], thus providing a clear experimental path for probing chiral superconductivity via electrical measurements. Similar DW phenomena can also be obtained in time-reversal-symmetric superconductors with opposite helical winding for each spin orientation of the Cooper pairs. This can occur in noncentrosymmetric superconductors with twin boundaries where helical edge modes [34–37] can drive nonstandard magnetic states and vortex configurations [38–40]. The observation of in-gap states surrounding topological superconducting domains in a single atomic layer of Pb covering magnetic islands [41] highlights the relevance of inhomogeneous topological states to evaluate the nature of the pairing and the role of magnetism.

It is well established that, due to the bulk-boundary correspondence, edge modes in topological superconductors appear when they are put in contact with conventional materials. Spin and charge currents, as well as spontaneous magnetic moments, have been predicted to occur at the boundary of

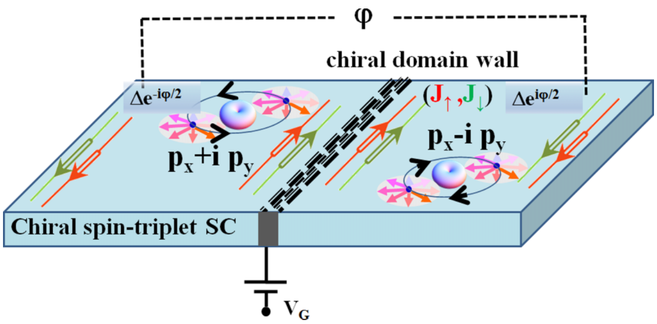

FIG. 1. Schematic view of the chiral domain wall structure made of two interfacing chiral spin-triplet superconductors with opposite windings. We depict representative d_z-vector configurations corresponding to a nonzero superconducting triplet order parameter and zero total spin projection along the z direction in the spin space, thus implying that the parallel-spin Cooper pairs lie in the xy plane, as schematically indicated by the magenta arrows. The domain wall is denoted by a black dashed line to separate the two regions with opposite windings of the superconducting order parameter for each spin direction. The arrows (green and red for up and down spins, respectively) along the domain wall stand for the spin-dependent charge currents due to the chiral symmetry of the superconductor and the presence of Andreev bound states. The $i_x = 0$ position labels the interface site between the two chiral domains. Each chiral domain has a finite size of $(L_x/2) \times L_y$ sites. For our simulation we assume that $L_x = L_y = 120$. Gating through V_G results in electrically tuning the effective interface potential amplitude U by suitably depleting or increasing the electron density near the domain wall. The two superconducting domains feel opposite phases, which is modeled by a spatially dependent factor $\exp[\mathrm{sgn}(i_x) i\phi/2]$ which multiplies the spin-triplet order parameter.

topological spin-triplet superconductors [42] or to interface with spin-singlet superconductors [43]. Their behavior is characterized by a remarkable dependence on the nature of the pairing interaction and of the interface potentials [42] and can be controlled by the phase difference across the interface [43]. At the same time, the effect of the domain walls on the properties of such heterostructures can lead to nonstandard transverse charge and spin currents across the chiral superconductor which are sensitively dependent on the parity of the number of chiral domain walls [44]. In particular, while it has been shown that at the interface between a spin singlet and a chiral spin triplet the Andreev states can be spin polarized along a direction that depends on the singlet-triplet mixing and on the phase relation, the possibility of designing an effective exchange coupling between such magnetic configurations has not been addressed before.

The aim of this paper is therefore to investigate the character of the magnetic Andreev states occurring near a chiral domain wall inside the spin-triplet superconducting region and to evaluate how they get coupled once electronic charge transfers are allowed and varied across the DW. We demonstrate that it is possible to achieve practical control of the resulting magnetic state by employing both the superconducting phase difference between the two chiral domains and an electric gating at the interface which controls the effective tunnel barrier strength by suitably depleting or increasing the electron density near the domain wall. The response of the resulting chiral DW superconducting planar junction, schematically depicted in Fig. 1, is analyzed by scanning the amplitudes of the electric and phase control parameters. Since the chiral spin-triplet states can have edge modes with spontaneous magnetization, different types of spin configurations can occur close to the chiral interface which are intimately connected to the local inversion symmetry breaking that drives the formation of parity mixing. The emerging physical scenario can be very rich, with a magnetization profile with variable amplitude and spin polarization with different orientations that can be tuned by the phase difference or by the electric gating. The domain wall then directly controls the amplitude and the relative orientations of the spin polarization forming at the two sides of the chiral domain wall. Moreover, in some cases, with weak interface potential, we find that the magnetization is pinned exactly at the domain wall, while in other circumstances, for larger electron density depletion, the spin polarization develops maximal amplitudes away from the chiral interface with a relative orientation that depends on the interface potential and the phase difference. We explore these possibilities and present a detailed analysis of the behavior of the magnetization in each configuration. We think that these realizations may pave the way to the possibility of having an inhomogeneous switchable functional topological superconductor with a distinct amplitude, orientation, and spatial profile of the magnetization developing in its interior in proximity to the chiral domain walls. Furthermore, these effects provide a remarkable and quite unique manifestation of phase-coherent and electric control of magnetic states in topological superconducting states.

This paper is organized in the following way. Section II is devoted to the introduction of the microscopic model describing the order parameter and electronic states of a chiral DW junction and to the methodology adopted to determine its magnetic and electrical properties. In Sec. III the results for the behavior of the magnetization close to the chiral interface are presented and discussed. Finally, the last section is devoted to the conclusions.

II. MODEL AND METHODOLOGY

We consider a planar chiral DW junction of size $L \times L$ (in units of the lattice constant) extending in the x-y plane, where the interface separating the two p-wave spin-triplet superconductors with opposite chiral windings is assumed to be parallel to the y direction (see Fig. 1). For simplicity we choose chiral domains of equal width, so that, if we denote the lattice sites by $\mathbf{i} \equiv (i_x, i_y)$, with i_x and i_y being integers between $-L/2$ and $L/2$, the domain wall is located at $i_x = 0$. Asymmetry of the chiral DW junction geometry does not qualitatively affect the physical behavior of the heterostructure, leaving unchanged our general conclusions. Hence, the sites $(0, i_y)$ along the domain wall define the boundary separating the two chiral domains.

The Hamiltonian is defined as

$$H = H_0 + H_S + H_T, \tag{1}$$

with

$$H_0 = \sum_{\langle \mathbf{i},\mathbf{j}\rangle,\sigma} t_{\mathbf{i},\mathbf{j}}(c^\dagger_{\mathbf{i}\sigma}c_{\mathbf{j}\sigma} + \text{H.c.}) - \mu \sum_{\mathbf{i}\in S,\sigma} n_{\mathbf{i}\sigma},$$

$$H_I = \sum_{\mathbf{i}} U(i) n_{\mathbf{i}},$$

$$H_T = \sum_{\langle \mathbf{i},\mathbf{j}\rangle} V_{\uparrow\downarrow}(n_{\mathbf{i}\uparrow}n_{\mathbf{j}\downarrow} + n_{\mathbf{i}\downarrow}n_{\mathbf{j}\uparrow}), \tag{2}$$

where H_0 contains the single-particle terms, H_T describes pairing in the spin-triplet chiral domains, and H_I is the interface charge potential. Here, $c_{\mathbf{i}\sigma}$ is the annihilation operator of an electron with spin σ at site $\mathbf{i}$, $n_{\mathbf{i}\sigma} = c^\dagger_{\mathbf{i}\sigma}c_{\mathbf{i}\sigma}$ is the corresponding number operator, μ is the chemical potential, and $t_{\mathbf{ij}}$ is the hopping amplitude, assumed to be nonvanishing only between nearest-neighbor sites $\langle \mathbf{i},\mathbf{j}\rangle$. Periodic boundary conditions are assumed only in the y direction since the presence of the interface separating the two domains breaks the translational symmetry along x. The short-range nearest-neighbor attractive interaction $-V_{\uparrow\downarrow}$ ($V_{\uparrow\downarrow} > 0$) allows for both singlet and triplet pairing channels with zero spin projection along the z axis. $U(i_x)$ is a lattice-dependent charge potential that effectively mimics the level of electronic matching across the domain wall between the two chiral regions. It may simulate the effect of an electric field applied on the chiral domain wall, allowing us to control the electron density occupation close to the interface. In order to describe the different electronic distributions we assume that $U(i_x)$ is uniform along y and it has a maximal amplitude U at the position of the domain wall, decreasing with a characteristic length away from the interface. The results are obtained with a Gaussian profile and a width $u_s = 6$ in units of the atomic distances. Other profiles for the interface charge potential do not qualitatively affect the results. Since we deal with magnetic effects at the singlet-triplet interface, it is convenient to introduce the local spin density polarization $\vec{s}(\mathbf{i}) = \sum_{s,s'} c^\dagger_{\mathbf{i}s}\vec{\sigma}_{s,s'}c_{\mathbf{i}s'}$ and the averaged total magnetization at a given position i_x along the x direction $\vec{S}(i_x) = \frac{1}{Ly}\sum_{i_y}\sum_{s,s'}\langle c^\dagger_{i_x i_y s}\vec{\sigma}_{s,s'}c_{i_x i_y s'}\rangle$. Thus, the total magnetization in a given region is simply the sum of $\vec{S}(i_x)$ over the sites of that region. We point out that the chiral edge states at the domain wall boundary can support net charge and spin currents whose spin character depends on the nature of the magnetic profile.

For the computational study of the superconducting state, the pairing interaction in the Hamiltonian in Eq. (1) is decoupled within the Hartree-Fock approximation as

$$V^{\sigma\sigma'} n_{\mathbf{i}\sigma}n_{\mathbf{j}\sigma'} \simeq V^{\sigma\sigma'}\left(\Delta^{\sigma\sigma'}_{\mathbf{ij}}c^\dagger_{\mathbf{j}\sigma}c^\dagger_{\mathbf{i}\sigma'} + \bar{\Delta}^{\sigma\sigma'}_{\mathbf{ij}}c_{\mathbf{i}\sigma'}c_{\mathbf{j}\sigma} - \left|\Delta^{\sigma\sigma'}_{\mathbf{ij}}\right|^2\right),$$

where the pairing amplitude on a given bond between electrons with spins σ and σ' at sites $\mathbf{i}$ and $\mathbf{j}$ is expressed by $\Delta^{\sigma\sigma'}_{\mathbf{ij}} = \langle c_{\mathbf{i}\sigma}c_{\mathbf{j}\sigma'}\rangle$. The numerical solution of the present problem consists of evaluating self-consistently these pair correlation amplitudes until we reach the ground-state configuration with the desired accuracy and, for the $S_z = 0$ sector, combining them to yield the spin-singlet and -triplet components as $\Delta^{S,T}_{\mathbf{ij}} = (\Delta^{\uparrow\downarrow}_{\mathbf{ij}} \pm \Delta^{\uparrow\downarrow}_{\mathbf{ji}})/2$. The solution is obtained by solving the Bogoliubov–de Gennes equations related to the Hamiltonian in Eq. (1) on the lattice [16,45], with the aim being to get the energy spectrum of the system, the spatially resolved spin polarization, and the Andreev states at the boundary of the superconductor and close to the chiral DW.

The spin-triplet order parameter is typically expressed in a matrix form [46] through the $\vec{d}$-vector components that are related to the pair correlations for the various spin-triplet configurations with zero spin projection along the corresponding symmetry axis. For the present investigation, the pairing interaction V is assumed to be nonzero only in the $\uparrow\downarrow$ channel, thus implying that the $\vec{d}$ vector is along z (Fig. 1). Importantly, near the interface, due to the inversion symmetry breaking along the x direction, the triplet order parameter gets mixed with the singlet component within the $S_z = 0$ channel. In the following, to simulate the chiral domain structure depicted in Fig. 1 we will consider that the triplet vector $\vec{d}_{\boldsymbol{p}}$ is $\vec{d} \equiv (0, 0, p_x + ip_y)$ for $i_x < 0$ and $\vec{d} \equiv (0, 0, p_x - ip_y)$ for $i_x > 0$. This solution can be enforced by requiring at the start of the self-consistent computation that the p_y component has opposite signs on the two sides of the interface. Moreover, to investigate the effects of the phase difference between the two chiral regions of the superconductor, we follow the conventional procedure employed for the study of the Josephson junctions by transforming the pairing wave function on the left and right sides of the heterostructure by the phase factors $\exp[-i\phi/2]$ and $\exp[i\phi/2]$, respectively (see Fig. 1). The initial step-function spatial dependence of the phase profile evolves into a smooth gradient across the domain wall in a region of the order of the coherence length for the ground state, as we have verified in the employed self-consistent scheme of computation (see the Appendix for more details). According to the chosen amplitude of the pairing strength, the coherence length for the heterostructure is of the order of 15–20 in units of the atomic distance, as shown in the Appendix. Concerning the domain wall configuration, we assume that it is spatially pinned and its structure is fixed. In principle, it can have a dynamical behavior and gets depinned in the presence of supercurrent or other external perturbations. This motion can modify the phase profile and also its resulting magnetic profiles due to spin-polarized Andreev states. This analysis will be addressed in a future work.

III. RESULTS

We start by discussing the magnetic phase diagram reported in Fig. 2. The analysis has been performed by varying the phase difference across the chiral domain wall and the strength of the charge potential at the chiral interface. The self-consistent spatial profile of the triplet and singlet order parameters near the chiral domain is sensitive to these control parameters and in turn determines the character of the Andreev spectra and of the magnetization. It is known [42] that the singlet-triplet inhomogeneous mixing at the boundary of a chiral spin-triplet superconductor can lead to a spin splitting of the chiral edge modes that yield a spontaneous magnetization together with spin currents flowing along the edge. Hence, for a chiral domain, the local breaking of inversion symmetry is a natural source of singlet-triplet mixing close to the wall. Such mixing is strongly dependent on the degree of electronic

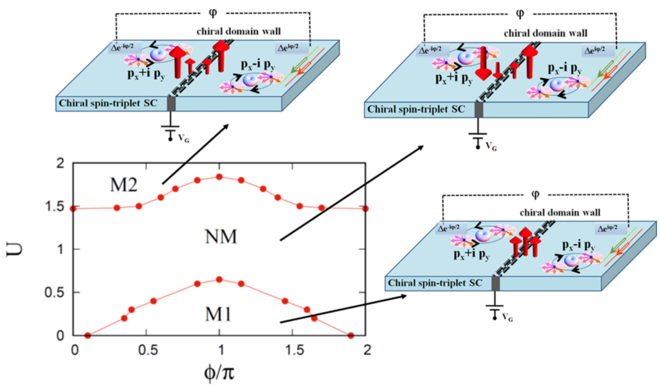

FIG. 2. Phase diagram of the most favorable magnetic configurations as a function of the applied phase difference across the chiral domain wall and of the interface potential U (in units of the planar hopping amplitude in the superconductor). M1 denotes a magnetic state with a small net spin polarization pinned at the domain wall position. NM stands for a vanishing average magnetization with opposite orientations on the two sides of the chiral interface. Finally, M2 denotes a state with a magnetization profile exhibiting a nonvanishing net spin moment with a maximal amplitude away from the domain wall at a characteristic distance which is of the order of the superconducting coherence length. Big red arrows schematically depict the amplitude and orientation of the spin polarization close to the chiral interface.

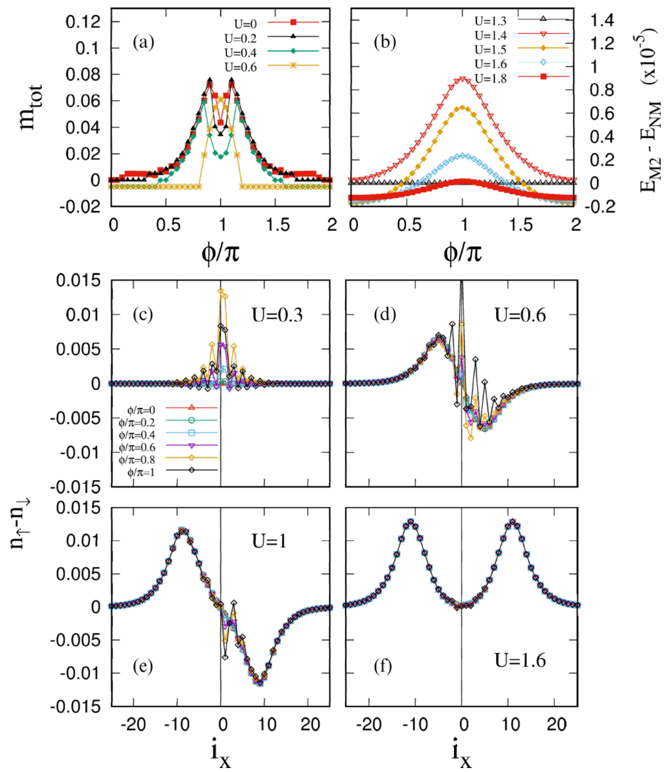

FIG. 3. (a) Integrated magnetization m_{tot} close to the chiral interface as a function of the superconducting phase difference ϕ between the two domains, assuming different amplitudes of the interface barrier potential U from 0 to 0.6 in units of the planar hopping value. (b) Evolution of the difference of the free energy associated with the magnetic (E_{M2}) and nonmagnetic (E_{NM}) configurations as a function of the superconducting phase drop ϕ and by varying the strength of the interface potential U towards a regime of significant electron density depletion at the chiral domain wall. (c)–(f) Spatial dependence of the magnetization (i.e., $n_\uparrow - n_\downarrow$) near the chiral domain wall (i.e., at $i_x = 0$) at different values of the phase drop across the chiral interface, moving from small to large potential amplitudes. For $U = 0.3$ [in (c)] a magnetization forms and is peaked at the position of the domain wall. The increase of the interface potential makes the spin polarization penetrating into the two chiral domains in an antiparallel configuration [in (d)], until a critical value of U is reached, above which the spin polarization acquires the same orientation on both domains.

matching between the two superconducting regions and, as expected, on the phase mismatch between the order parameters across the chiral wall. Indeed, on the basis of symmetry arguments, while a nonvanishing magnetization is expected to occur as a consequence of the nontrivial singlet-triplet mixing at the boundary of the superconductor, the phase relation between the singlet and triplet order parameters may affect the orientation of the spin polarization. Due to these competing effects, the chiral interface can exhibit rich magnetic properties. This is indeed one of the fundamental outcomes of the analysis summarized in the phase diagram of Fig. 2. We find three distinct magnetic states that occur close to the chiral domain wall. For a weak interface potential, the electronic matching between the two chiral regions is good, and the magnetic configuration, here denoted by M1, with a small net spin polarization pinned at the domain wall position has the same orientation in the whole region of the chiral interface, exhibiting the larger amplitude at the position of the chiral domain wall (i.e., $i_x \sim 0$). In such a regime, the application of a phase difference ϕ favors the M1 state allowing a maximal region of stability for $\phi = \pi$. On the contrary, without any external phase drop across the chiral domain wall, the M1 magnetic state cannot be achieved.

The increase of the interface potential U tends to deplete the electron density at the chiral domain wall and in turn leads to a magnetic transition from the M1 state to a configuration, denoted by NM, with a vanishing average magnetization with opposite orientations on the two sides of the chiral interface, which although globally nonmagnetic has distinctive magnetic marks. Indeed, it has a spatial modulation of the magnetization amplitude and orientation such that the spin polarization is antialigned on the two sides of the chiral interface. A further increase of the interface potential brings the topological interface into a regime of reduced charge transfer between the chiral domains. Remarkably, the NM magnetic state can be turned into a configuration M2 having a net nonvanishing spin polarization with a magnetization profile that is only amplitude modulated without any orientation change.

To make a deeper inspection of the achieved magnetic phases, we consider the details of the spatial profile of the magnetic configurations close to the chiral domain wall as a function of the phase difference across the chiral DW for representative values of the interface potential (Fig. 3). As already pointed out above, the M1 state has a net spin polarization which clearly emerges once we integrate the magnetization over the whole chiral interface. The integrated spin amplitude m_{tot} clearly shows the transition between the M1 and NM phases as a function of the phase difference ϕ [Fig. 3(a)]. We point out that the phase diagram has been inferred by explicitly computing the ground-state energy corresponding to the self-consistent solutions for the superconducting order parameters. Such an analysis is highlighted in Fig. 3(b), where we plot the evolution of the energy difference between the ground states associated with the NM and M2 phases.

The investigation of the spatial magnetization profile near the chiral interface is extremely useful to further characterize the various magnetic phases. We find that the M1 configuration is marked by a spin polarization that is pinned at the position of the chiral domain wall and rapidly decays when moving away from the interface [Fig. 3(c)]. This is expected in a regime of very good electronic matching so that a significant degree of hybridization occurs between the chiral edge modes. As shown in Fig. 3(d), the increase of the interface potential amplitude U remarkably makes the magnetic distribution gradually develop an antiparallel spin pattern on the two sides of the chiral interface, with antialigned components having a maximum at a characteristic distance from the interface which is of the order of the superconducting coherence length. We notice that the depletion of the electron density reduces the magnetization at the domain wall position, and the application of a nontrivial phase difference between the chiral domains sets further amplitude modulation of the spin polarization with an average spin profile that keeps the antiparallel pattern. These short-length-scale modulations are more pronounced for values of U close to the phase diagram boundary separating the M1 and NM configurations. Moving farther away from the transition regime, the spin antiparallel profile gets stabler, and the magnetization peaks grow in amplitude [Fig. 3(e)]. Finally, a further depletion of the electron density at the domain wall stabilizes a magnetic phase with parallel spin polarization on the two sides of the chiral superconductor [Fig. 3(f)]. This result clearly demonstrates a spin switching effect at the chiral domain wall with a transition from an antiparallel to parallel spin alignment across the wall. Moreover, due to the shape of the boundaries in the phase diagram of Fig. 2, the NM-M1 and NM-M2 transitions can be achieved by tuning either the superconducting phase difference or the strength of the interface charge potential U. Finally, we point out that due to the presence of spin-polarized chiral edge modes, there are charge and spin currents flowing along the chiral domain wall that may show different spatial profiles, depending on the magnetic configuration established in the system.

IV. CONCLUSIONS

We have determined the magnetic phase diagram of a chiral interface by considering a domain wall structure inside the chiral spin-triplet superconducting region. We have also investigated the dependence of the magnetic states on the phase difference across the DW and on an interface charge potential strength mimicking an effective electrical gating at the DW. Although the magnetization is always generated by a parity mixing induced by a local inversion symmetry breaking close to the domain wall, its character is strongly dependent on the phase and the electric drives. Remarkably, we demonstrated that for chiral superconductors with $S_z = 0$ opposite spin-triplet pairing, the interface magnetization normal to the plane can be switched from a parallel to antiparallel configuration by varying the phase difference ϕ across the wall and the amplitude of the charge transfer between the chiral domains. This suggests a possible realization of quite unique systems which can be employed to store elemental information in spin-polarized states attached to topological defects.

It is also useful to discuss the possible experimental means to achieve electrical control of the domain wall interface potential. We start by observing that the possibility to achieve an electric gating at the interface of the chiral domain mainly applies to thin films or two-dimensional superconductors. Moreover, one can expect that the formation and the pinning of a chiral wall to be more favorable in a region of the superconductor where impurities or defects may accumulate, giving rise to a spatial variation of the superconducting order parameter. Indeed, since we are dealing with the formation of a chiral domain wall, a spatial variation of the superconducting order parameter is an important prerequisite for its nucleation. Then, close to the chiral interface, it is more favorable that the superconducting state is suppressed, also as a consequence of the chiral change across the interface of the component of the order parameter parallel to the wall. This is, indeed, consistent with the output of our analysis. Therefore, the electronic states close to the domain wall, especially due to the presence of disorder or electronic inhomogeneities and owing to confining potentials related to the structure of interface, are prone to form localized configurations which are thus poorly conducting. The resulting scenario corresponds to effective inhomogeneous electronic states near the chiral interface that are poorly itinerant and form a barrier separating the two superconducting chiral domains. These states, in turn, determine the amplitude of the potential U introduced in our electronic modeling and are responsible for the character and strength of the charge transfer processes across the interface. In such circumstances, since a static electric field is screened in a superconductor on the atomic length scale (Thomas-Fermi length), the effects of the electric field will mainly manifest at the interface of the superconducting chiral domains on the electronic states that form in the region where the superconducting order parameter is dominantly suppressed.

From an experimental point of view, an efficient way of applying a local electric field in the spatial region where the chiral domain wall is formed would be to employ the so-called ionic liquid technique. An ionic liquid consists of ions and forms electric double layers at the interfaces with the electrodes when a voltage is applied across the ionic liquid. One layer consists of anions or cations of the ionic liquid, while the other layer includes the induced charge carriers of the solid. Depending on the nature of the electronic states in the electrically driven materials, charge carrier densities of up to 8×10^{14} cm^{-2} can be obtained [47] with a separation within the double layer of about 1 nm. Such an approach has been successfully employed to induce insulator-to-superconductor transitions in oxide-based superconductors [48,49], and metal-to-insulator transitions in two-dimensional systems [50] or Mott insulators [51]. Recently, studies of two-dimensional (2D) or quasi-2D materials have indicated that ionic liquid gating can either induce superconductivity or give access to a complete set of competing electronic phases [52–54]. It is also worth pointing out that recent experimental achievements have demonstrated the possibility

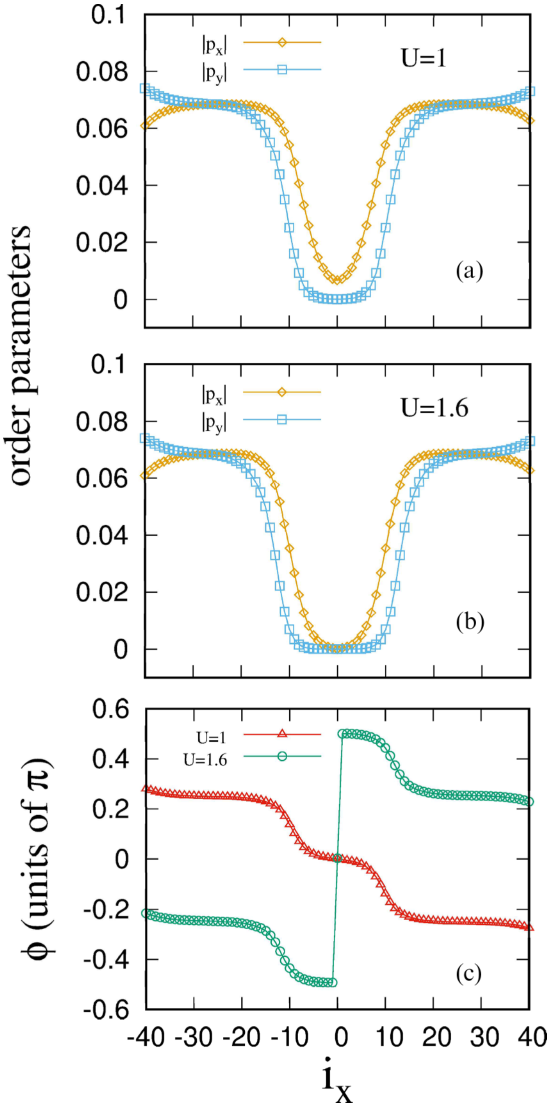

FIG. 4. Spatial profile of (a) and (b) the amplitude and (c) phase of the superconducting order parameters in the proximity of the chiral domain wall for two representative values of the interface potential. The values $U = 1$ and $U = 1.6$ correspond to phases NM and M2, respectively.

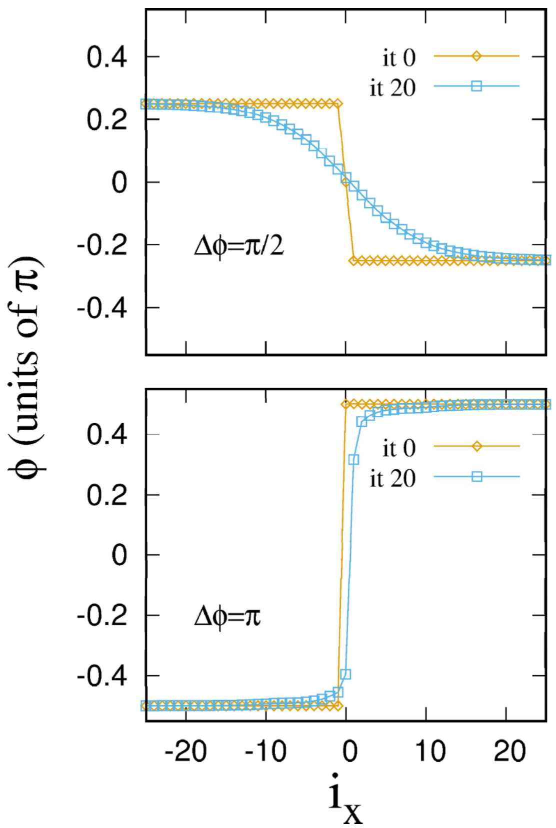

FIG. 5. Spatial dependence for $U = 1$ of the phase of the superconducting order parameter close to the domain wall considering for the applied phase difference $\Delta\phi$ the input step-function profile ($it = 0$) and the one obtained after a number $it = 20$ of iterations. Two values of $\Delta\phi$ are considered, i.e., $\Delta\phi = \pi/2$ (top panel) and $\Delta\phi = \pi$ (bottom panel).

to electrostatically tune the superconducting state of conventional superconductors, such as Ti and Al, in the regime of thin-film thickness comparable with the superconducting coherence length [55,56]. On the basis of such considerations, although not applicable to all superconducting materials, one can envisage various feasible paths for an electrical control of chiral interfaces which are especially suitable for 2D or quasi-2D superconducting systems.

ACKNOWLEDGMENTS

We acknowledge valuable and fruitful discussions with I. Vekhter. M.C. acknowledges support from the project QUANTOX of QuantERA ERA-NET Cofund in Quantum Technologies (Grant Agreement No. 731473), implemented within the EU H2020 program.

APPENDIX

In this Appendix, in order to estimate the effective coherence length of the simulated superconducting state and the possible reconstruction of the order parameter in the presence of an applied phase difference, we present its spatial profile for both amplitude and phase close to the chiral interface. The analysis is performed for two representative values of the charge potential U corresponding to antiparallel (NM) and parallel (M2) spin polarizations of the Andreev states in proximity to the domain wall (see Fig. 4). One can notice that for both the NM and M2 phases, the amplitude of the order parameter rapidly varies close to the chiral interface, then reaches a constant profile in the inner side of the superconductor within a spatial window which sets the size of the effective coherence length. This is a standard procedure for assessing the amplitude of the coherence length of a given superconducting state, and similar estimates are obtained in our study when the behavior of the pairing amplitude is analyzed in proximity to the interface with the vacuum on the other edges of the heterostructure. Hence, for the selected values of the pairing strength, the coherence length of the superconductor is of the order of 15–20 lattice constants. A change in the pairing interaction generally leads to a modification of the coherence length. We have verified that the results of the domain wall spin reconstruction are not qualitatively affected by modification of the pairing coupling and, in turn, of the coherence length.

Furthermore, as expected on the basis of the nature of the chiral domain, since the p_y component of the order parameter has to change sign across the domain wall, its amplitude tends to vanish more rapidly than the p_x component [Figs. 4(a) and 4(b)]. On the other hand, the p_x component is more sensitive to the strength of the interface charge potential U and, due to the breaking of translational invariance and the presence of the domain wall, is also suppressed in the proximity of the chiral interface. Concerning the spatial profile of the intrinsic phase of the superconducting state, since we are dealing with a two-component order parameter, we can determine the relative phase between the p_x and p_y components at a given position on each side of the heterostructure. Indeed, writing the order parameter in the form $\Delta_p(i_x) = p(i_x)\exp[i\phi(i_x)]$, with $p(i_x) = \sqrt{p_x(i_x)^2 + p_y(i_x)^2}$ and $\phi(i_x) = \arctan[p_y(i_x)/p_x(i_x)]$, we find that in the NM phase the intrinsic phase smoothly changes sign when moving from the left to the right side of the chiral interface. The value of the phase of about $-\pi/4$ to $\pi/4$ is consistent with the fact that the amplitudes of p_x and p_y are comparable in the inner side of the superconducting domain. Moreover, since the p_y component is more significantly suppressed than the p_x one close to the interface, the intrinsic phase relation is vanishing in that region. A different behavior is obtained in the case of the M2 state, where an additional $\pi/2$ phase with opposite sign is acquired on the two sides of the chiral interface. This implies that there is a nontrivial intrinsic π shift across the domain wall which makes the spin-polarized phase an effective π junction, as one would expect in the case of a heterostructure made by connecting two superconductors through a ferromagnetic interface. Due to the vanishing amplitude of the p_y component, it is the p_x part which acquires a $\pi/2$ phase to allow a modification of the spin polarization across the domain wall. The chiral behavior of the system is confirmed by the opposite sign of the phase away from the domain wall.

Another aspect to address when considering the application of a phase difference on the two sides of the heterostructure is how the spatial profile of the phase readjusts in proximity to the domain wall. As we mentioned in the Sec. II, it is standard practice for the study of a Josephson effect to apply a phase difference across the junction by introducing the phase factors $\exp[-i\phi/2]$ and $\exp[i\phi/2]$ with a step-function profile. However, this phase configuration with an abrupt jump at the wall position $i_x = 0$ cannot represent an equilibrium state. Indeed, in our calculation, after having determined the ground-state configuration of the amplitude of the order parameter, we also consider the spatial reconstruction of the phase by an iterative procedure. The typical outcome when dealing with the phase gradient is that the phase smoothly evolves across the interface and tends to the value of the applied phase difference far from it. In Fig. 5 we report the behavior of the phase difference for an interface potential $U = 1$ and two choices of the applied phase difference. The procedure consists of introducing a step-function profile at step 0 ($it = 0$) and then to iterate for a given number of steps until reaching a physically relevant profile for the phase gradient. For our purposes a number of iterations with $it = 20$ are sufficient to achieve the targeted configuration.

[1] M. Sigrist and K. Ueda, Rev. Mod. Phys. **63**, 239 (1991).

[2] Y. Tanaka, T. Hirai, K. Kusakabe, and S. Kashiwaya, Phys. Rev. B **60**, 6308 (1999).

[3] N. Read and D. Green, Phys. Rev. B **61**, 10267 (2000).

[4] D. A. Ivanov, Phys. Rev. Lett. **86**, 268 (2001).

[5] A. Y. Kitaev, Phys. Usp. **44**, 131 (2001).

[6] G. E. Volovik, *The Universe in a Helium Droplet* (Oxford University Press, Oxford, 2003).

[7] Y. Maeno, S. Kittaka, T. Nomura, S. Yonezawa, and K. Ishida, J. Phys. Soc. Jpn. **81**, 011009 (2012).

[8] M. Sato and Y. Ando, Rep. Prog. Phys. **80**, 076501 (2017).

[9] S. Murakami, N. Nagaosa, and M. Sigrist, Phys. Rev. Lett. **82**, 2939 (1999).

[10] E. Dumitrescu and S. Tewari, Phys. Rev. B. **88**, 220505(R) (2013).

[11] E. Dumitrescu, J. D. Sau, and S. Tewari, Phys. Rev. B. **90**, 245438 (2014).

[12] T. Hyart, A. R. Wright, and B. Rosenow, Phys. Rev. B **90**, 064507 (2014).

[13] M. T. Mercaldo, M. Cuoco, and P. Kotetes, Phys. Rev. B **94**, 140503(R) (2016).

[14] M. T. Mercaldo, M. Cuoco, and P. Kotetes, Phys. B (Amsterdam, Neth.) **536**, 730 (2018).

[15] M. T. Mercaldo, P. Kotetes, and M. Cuoco, AIP Adv. **8**, 101303 (2018).

[16] A. Romano, M. Cuoco, C. Noce, P. Gentile, and G. Annunziata, Phys. Rev. B **81**, 064513 (2010).

[17] K. Sengupta, I. Žutić, H.-J. Kwon, V. M. Yakovenko, and S. Das Sarma, Phys. Rev. B **63**, 144531 (2001).

[18] H.-J. Kwon, K. Sengupta, and V. M. Yakovenko, Low Temp. Phys. **30**, 613 (2004).

[19] G. Annunziata, M. Cuoco, C. Noce, A. Sudbø, and J. Linder, Phys. Rev. B **83**, 060508(R) (2011).

[20] P. M. R. Brydon, C. Iniotakis, D. Manske, and M. Sigrist, Phys. Rev. Lett. **104**, 197001 (2010).

[21] P. Gentile, M. Cuoco, A. Romano, C. Noce, D. Manske, and P. M. R. Brydon, Phys. Rev. Lett. **111**, 097003 (2013).

[22] K. Sengupta and V. M. Yakovenko, Phys. Rev. Lett. **101**, 187003 (2008).

[23] J. Linder and J. W. A. Robinson, Nat. Phys. **11**, 307 (2015).

[24] K. Ishida, H. Mukuda, Y. Kitaoka, K. Asayama, Z. Q. Mao, Y. Mori, and Y. Maeno, Nature (London) **396**, 658 (1998).

[25] A. P. Mackenzie and Y. Maeno, Rev. Mod. Phys. **75**, 657 (2003).

[26] C. Kallin, Rep. Prog. Phys. **75**, 042501 (2012).

[27] S. P. Mukherjee and K. V. Samokhin, Phys. Rev. B **91**, 104521 (2015).

[28] M. Matsumoto and M. Sigrist, J. Phys. Soc. Jpn. **68**, 994 (1999).

[29] J. R. Kirtley, C. Kallin, C. W. Hicks, E.-A. Kim, Y. Liu, K. A. Moler, Y. Maeno, and K. D. Nelson, Phys. Rev. B **76**, 014526 (2007).

[30] F. Kidwingira, J. D. Strand, D. J. V. Harlingen, and Y. Maeno, Science **314**, 1267 (2006).
[31] H. Kambara, S. Kashiwaya, H. Yaguchi, Y. Asano, Y. Tanaka, and Y. Maeno, Phys. Rev. Lett. **101**, 267003 (2008).
[32] M. S. Anwar, T. Nakamura, S. Yonezawa, M. Yakabe, R. Ishiguro, H. Takayanagi, and Y. Maeno, Sci. Rep. **3**, 2480 (2013).
[33] I. Serban, B. Béri, A. R. Akhmerov, and C. W. J. Beenakker, Phys. Rev. Lett. **104**, 147001 (2010).
[34] M. Sato and S. Fujimoto, Phys. Rev. B **79**, 094504 (2009).
[35] C. K. Lu and S. Yip, Phys. Rev. B **82**, 104501 (2010).
[36] Y. Tanaka, T. Yokoyama, A. V. Balatsky, and N. Nagaosa, Phys. Rev. B **79**, 060505(R) (2009).
[37] T. Yokoyama, Y. Tanaka, and J. Inoue, Phys. Rev. B **72**, 220504(R) (2005).
[38] C. Iniotakis, S. Fujimoto, and M. Sigrist, J. Phys. Soc. Jpn. **77**, 083701 (2008).
[39] H. Mukuda, S. Nishide, A. Harada, K. Iwasaki, M. Yogi, M. Yashima, Y. Kitaoka, M. Tsujino, T. Takeuchi, R. Settai, Y. Onuki, E. Bauer, K. M. Itoh, and E. E. Haller, J. Phys. Soc. Jpn. **78**, 014705 (2009).
[40] E. Arahata, T. Neupert, and M. Sigrist, Phys. Rev. B **87**, 220504(R) (2013).
[41] G. C. Ménard, S. Guissart, Ch. Brun, R. T. Leriche, M. Trif, F. Debontridder, D. Demaille, D. Roditchev, P. Simon and T. Cren, Nat. Commun. **8**, 2040 (2017).
[42] A. Romano, P. Gentile, C. Noce, I. Vekhter, and M. Cuoco, Phys. Rev. Lett. **110**, 267002 (2013).
[43] A. Romano, P. Gentile, C. Noce, I. Vekhter, and M. Cuoco, Phys. Rev. B **93**, 014510 (2016).
[44] A. Romano, C. Noce, I. Vekhter, and M. Cuoco, Phys. Rev. B **96**, 054512 (2017).
[45] M. Cuoco, A. Romano, C. Noce, and P. Gentile, Phys. Rev. B **78**, 054503 (2008).
[46] R. Balian and N. R. Werthamer, Phys. Rev. **131**, 1553 (1963).
[47] H. Yuan, H. Shimotani, A. Tsukazaki, A. Ohtomo, M. Kawasaki, and Y. Iwasa, Adv. Funct. Mater. **19**, 1046 (2009).
[48] X. Leng, J. Garcia-Barriocanal, S. Bose, Y. Lee, and A. M. Goldman, Phys. Rev. Lett. **107**, 027001 (2011).
[49] K. Ueno, S. Nakamura, H. Shimotani, H. T. Yuan, N. Kimura, T. Nojima, H. Aoki, Y. Iwasa, and M. Kawasaki, Nat. Nanotechnol. **6**, 408 (2011).
[50] Y. Saito and Y. Iwasa, ACS Nano **9**, 3192 (2015).
[51] K. Ueno, S. Nakamura, H. Shimotani, A. Ohtomo, N. Kimura, T. Nojima, H. Aoki, Y. Iwasa, and M. Kawasaki, Nat. Mater. **7**, 855 (2008).
[52] Y. Saito, Y. Kasahara, J. Ye, Y Iwasa, and T. Nojima, Science **350**, 409 (2015).
[53] S. Jo, D. Costanzo, H. Berger, and A. F. Morpurgo, Nano. Lett. **15**, 1197 (2015).
[54] L. J. Li, E. C. O'Farrell, K. P. Loh, G. Eda, B. Özyilmaz, A. H. Castro Neto *et al.*, Nature (London) **529**, 185 (2016).
[55] G. De Simoni, F. Paolucci, P. Solinas, E. Strambini, and F. Giazotto, Nat. Nanotechnol. **13**, 802 (2018).
[56] F. Paolucci, G. De Simoni, E. Strambini, P. Solinas, and F. Giazotto, Nano Lett. **18**, 4195 (2018).